Available online at www.sciencedirect.com
ScienceDirect
Journal of the European Ceramic Society 29 (2009) 2603–2610
www.elsevier.com/locate/jeurceramsoc

Thermal behaviour of $La_{0.8}Sr_{0.2}Fe_{1-x}Ga_xO_{3-\delta}$ ($x = 0$ or $x = 0.3$)

A. Julian [a,b], E. Juste [a,b], P.M. Geffroy [a,*], N. Tessier-Doyen [c], P. Del Gallo [b], N. Richet [b], T. Chartier [a]

[a] CNRS-ENSCI, SPCTS, 47 avenue Albert Thomas, 87065 Limoges, France
[b] Air Liquide, Centre de Recherche Claude-Delorme, 1 chemin de la porte des Loges, Les Loges-en-Josas, B.P. 126-78354 Jouy-en-Josas Cedex, France
[c] GEMH, ENSCI, 47 avenue Albert Thomas, 87065 Limoges, France

Received 2 October 2008; received in revised form 19 February 2009; accepted 26 February 2009
Available online 24 April 2009

Abstract

The thermo-mechanical behaviours of $La_{0.8}Sr_{0.2}Fe_{1-x}Ga_xO_{3-\delta}$ ($x = 0$ or $x = 0.3$) ceramics for catalytic membrane reactors are studied up to 1100 °C under air and nitrogen atmospheres. XRD data, thermogravimetric and dilatometric analyses associated with Young's modulus measurements give a better understanding and a qualitative description of the mechanical behaviour of the perovskite materials as a function of temperature. First, a decrease of Young's modulus from room temperature to 300–400 °C is attributed to FeO_6 octahedrons distorsions of the monoclinic (or orthorhombic) phase. After phase transition, the rhombohedral phase exhibits a higher TEC and a stiffening of the perovskite structure probably due to less distorted FeO_6 octahedrons. Finally, at higher temperatures ($T > 800$ °C), thermogravimetric data show a weight loss attributed to oxygen departure from the perovskite structure leading to a large cell expansion.

This study presents the structural evolution of both materials and its impact on the thermal and mechanical behaviours that have to be considered for industrial uses.

Keywords: Perovskites; Thermal expansion; Membranes; X-ray methods; Young's modulus

1. Introduction

The interest for catalytic membrane reactors (CMR) has greatly increased since they were found to allow conversion of natural gas to synthesis gas (CO and H_2 mixture) with a better efficiency and a lower cost than conventional processes.[1–3] These reactors make it possible to separate oxygen from air and to achieve conversion of methane, in a single step, by means of a mixed ionic/electronic conducting membrane. However, the ceramic membrane material should meet many requirements such as high oxygen permeation rate, long-range thermal and chemical stability under a large range of oxygen partial pressure, corresponding typically to membrane reactors conditions,[3] and suitable mechanical properties for industrial applications. One promising group of membrane materials is ABO_3 perovskite-type oxide such as (La, Sr)(Fe, Ga)$O_{3-\delta}$.

Nevertheless, previous studies have shown that self supported thick membranes cannot reach a high enough oxygen flux to compete with traditional syngas production routes, i.e. steam methane reforming and auto-thermal reforming. Oxygen flux can be significantly improved by decreasing the membrane thickness and adding a catalyst layer. In this way, the co-firing of a CMR consisting of a thick porous support and a thin dense membrane seems to constitute a good solution to meet this requirement.[4–12] The porous support provides suitable mechanical properties, while the dense membrane separates oxygen from air by ionic oxygen conduction. A catalyst layer can be added to improve the surface exchange and the conversion of methane on the surface of the membrane.

The elaboration by co-firing requires a good knowledge of the thermo-mechanical properties of the materials. For instance, a large thermal expansion coefficient (TEC) mismatch between the porous support and the dense membrane can lead to cracking and finally destruction of the reactor. In this respect, this study presents the thermo-mechanical properties of both materials of the dense and porous layers, over a large range of temperature and atmosphere in order to be as close as possible to the

* Corresponding author. Tel.: +33 5 55 45 22 65; fax: +33 5 55 79 69 54.
E-mail address: pierre-marie.geffroy@unilim.fr (P.M. Geffroy).

0955-2219/$ – see front matter © 2009 Elsevier Ltd. All rights reserved.
doi:10.1016/j.jeurceramsoc.2009.02.016

Table 1
Characteristics of powders.

Powder	d_{50} (μm)	Specific surface area (m^2/g)
LSFG 8273	0.26	10
LSF 821	0.40	7

working conditions. The aim of our approach is to evaluate the mechanical reliability of the membrane in working conditions, as proposed by Blond and Richet.[13]

$La_{0.8}Sr_{0.2}Fe_{0.7}Ga_{0.3}O_{3-\delta}$ material has been selected for the dense membrane, because of the high performance in terms of oxygen permeation and a good chemical and dimensional stability over a large range of temperature and oxygen partial pressure.[5,6,9,10] However, gallium-doped ferrites are very expensive due to the cost of Ga.

The selected material for the porous support is also a perovskite to prevent chemical interaction with the dense membrane, but without gallium to decrease the cost of the CMR. The proposed material is $La_{0.8}Sr_{0.2}FeO_{3-\delta}$.

2. Experimental

2.1. Samples preparation

$La_{0.8}Sr_{0.2}Fe_{0.7}Ga_{0.3}O_{3-\delta}$ and $La_{0.8}Sr_{0.2}FeO_{3-\delta}$ respectively denoted LSFG 8273 and LSF 821 were synthesized by spray pyrolysis (Pharmacie Centrale de France, France). Powders were calcined at 1000 °C in air respectively during 6 and 2 h before an attrition milling step. Specific surface area and mean grain size after milling are reported in Table 1.

Samples were elaborated by tape-casting which is currently used to produce thin ceramic films. The preparation of the suspensions was described in a previous paper.[14] The suspensions are degassed and directly cast onto a siliconed Mylar carrier film with a doctor blade. After solvent evaporation at room temperature under air, the obtained green tapes with a thickness of 150 μm are easily handled. Disks of 30 mm of diameter were punched from the green tapes, stacked and laminated at 85 °C under a pressure of 50 MPa.

Rectangular bars (40 mm × 3 mm × 3 mm) for Young's modulus measurements were pressed. The powders were previously planetary milled in an organic solvent (mixture of butanone-2 and ethanol in the azeotropic proportion) with a dispersant (phosphoric ester 1 wt.%), a binder (acrylic resin 3 wt.%) and a phthalate plasticizer (1 wt.%) during 4 h. After drying, the formulations were granulated through a 250 μm mesh sieve and the granules obtained were uniaxially pressed under 100 MPa.

All samples are debinded at 650 °C and sintered at 1250 °C during 2 h in air with a slow cooling rate (i.e. 2 °C/min) to reach an equilibrium with the surrounding atmosphere.

2.2. Sample characterizations

LSFG 8273 as a dense membrane material for catalytic membrane reactor must exhibit the lowest possible porosity in order to avoid gas leakage through the membrane. Relative densities of sintered samples were evaluated at 98% for tape-cast samples and at 96% for pressed samples, using Archimedes' method and helium pycnometry. Fractures of sintered samples prepared by die-pressing revealed submicronic closed pores (Fig. 1).

The crystallographic phases of LSFG 8273 were followed in air and nitrogen between 25 °C and 900 °C by X-ray diffraction (XRD) using a Bruker D8 with Cu Kα radiation. Crystallographic structure of LSF 821 at room temperature was determined by XRD (INEL CPS 120). Lattice parameters were refined using the full-profile Rietveld method. All XRD measurements were performed on powders treated at 1250 °C during 2 h in air.

Thermal expansion was measured by dilatometry (SETARAM setsoft 2400) on 10 mm long samples extracted from sintered laminated stacks. Measurements were performed

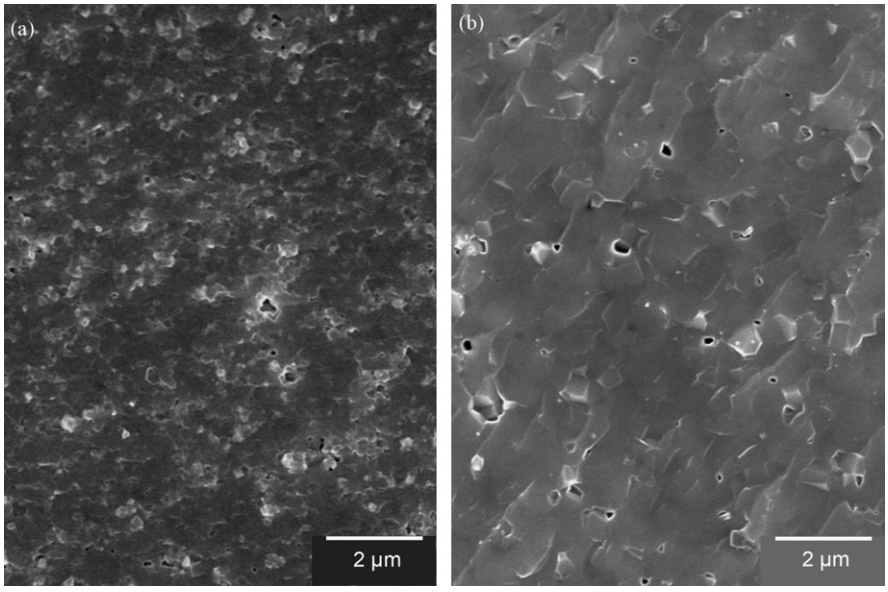

Fig. 1. SEM observations of unpolished cross sections of (a) LSFG 8273 and (b) LSF 821 pressed and sintered samples.

Table 2
Lattice parameters and cell volume of heat treated powder at room temperature.

	Space group	a (Å)	b (Å)	c (Å)	β (°)	V (Å^3)
LSFG 8273	Monoclinic P2/m	7.81_7	5.54_7	5.52_7	90.10 (±0.01°)	239.64
LSF 821	Orthorhombic Pbnm	5.54_9	5.52_9	7.81_1	–	239.99

under air and nitrogen flow (30 ml/min) with a heating rate of 4 °C/min from room temperature to 1100 °C. For thermogravimetric analyses, disks punched from green tapes were sintered, then crushed into powder. Measurements were performed under air and argon with a heating and cooling rate of 4 °C/min using a SETARAM setsys apparatus.

A high temperature ultrasonic pulse echo technique (350 kHz) was used to measure the evolution of Young's modulus (E) from 20 °C to 1100 °C.[15] Heating and cooling rates were 4 °C/min and 2 °C/min respectively.

3. Results and discussion

3.1. Structural analysis

At room temperature, LSF 821 material could be indexed as an orthorhombic phase (Pnma)[16,17] and LSFG 8273 material as a monoclinic phase (P2/m). Lattice parameters of the two materials at room temperature are reported in Table 2. The space group has an influence on the distortion of the perovskite cell and particularly on the octahedral tilt ($a^+b^-b^-$ for the orthorhombic phase and $a^+b^-c^-$ for the monoclinic phase in Glazer notation).[18] The data obtained by XRD show that the presence of Ga^{3+} on the B-site of the perovskite involves a distortion of the perovskite cell and so a tilting of the octahedron.

Table 3
Thermal expansion coefficients of individual lattice parameter of the monoclinic phase (20–200 °C).

Lattice parameter	TEC (°C^{-1}) (air)
a	14.1×10^{-6}
b	13.1×10^{-6}
c	7.04×10^{-6}

The Ga doping also has a direct effect on BO_6 octahedrons. In LSF 821, all Fe–O bond distances are similar, whereas for LSFG 8273 different Ga–O and Fe–O bond lengths are increasing the octahedron distortion.

On heating, LSFG 8273 exhibits similar behaviours in air ($pO_2 = 0.21$ atm) and nitrogen ($pO_2 = 10^{-5}$ atm) atmospheres. From room temperature to 200 °C, only the monoclinic phase is present (Fig. 2a and c). The thermal expansion coefficient values of the three lattice parameters of the monoclinic phase were calculated from XRD data and are reported in Table 3. It can be noted that there is a great anisotropy in the evolution of the lattice parameters; the TECs of the a- and b-lattice parameters are similar and twice as high as those of the c-lattice parameter. This results in an elongation of Fe_1–O_2 and Fe_1–O_3 bonds larger than for Fe_1–O_1 bond, as can be seen on the schematic view of the monoclinic structure in Fig. 3. Consequently, this anisotropy

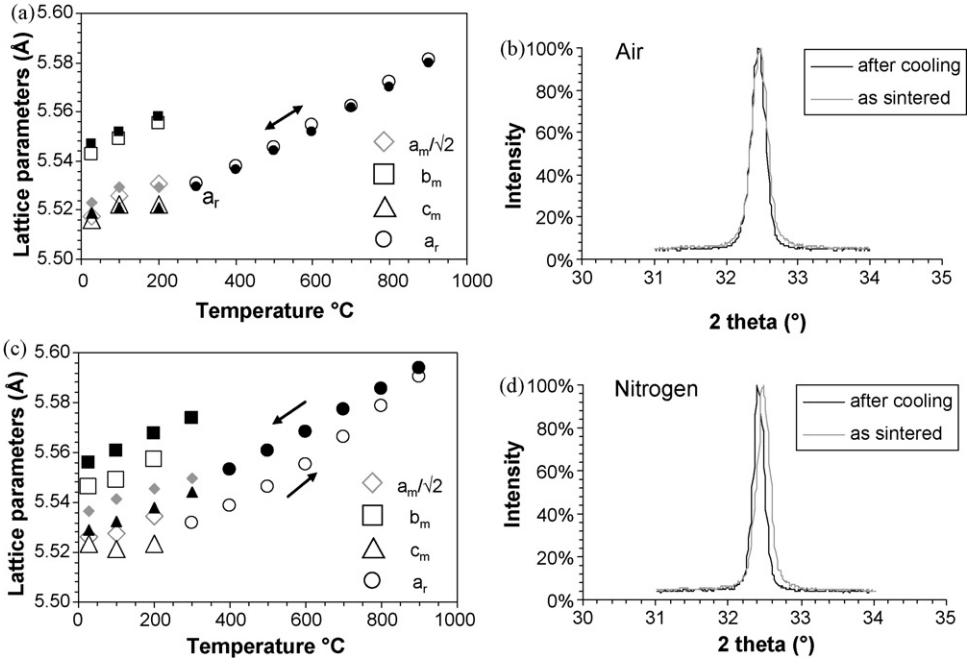

Fig. 2. High temperature XRD of LSFG 8273 under (a and b) air and (c and d) nitrogen from room temperature to 900 °C (m is for monoclinic phase and r for rhombohedral phase, open symbols correspond to heating and solid symbols to cooling).

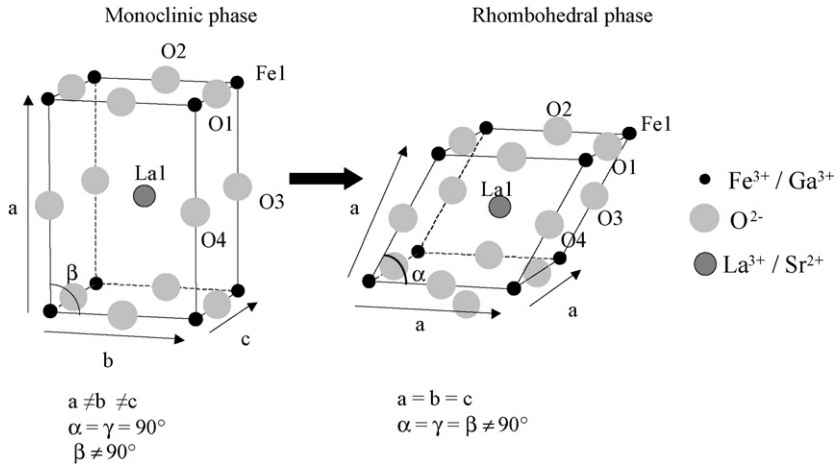

Fig. 3. Schematic view of phase transition of LSFG 8273. Octahedral tilting is not considered.

implies an increase of the distortion of BO_6 octahedrons over this range of temperature, i.e. from room temperature to 200 °C.

Then between 200 °C and 300 °C, a phase transition from monoclinic to rhombohedral (R-3c) symmetry occurs, implying a different tilt system of the octahedron ($a^-a^-a^-$). As the rhombohedral phase is reached, Fe_1–O_1, Fe_1–O_2 and Fe_1–O_3 bonds become equal resulting in a less distorted BO_6 octahedron (Fig. 3).

After 650 °C, an increase in cell volume is noted, with a more important increase in nitrogen than in air. It is well known that thermal expansion of perovskite materials is strongly dependent on the surrounding atmosphere at high temperature. This can be correlated to a larger oxygen departure from the perovskite structure in nitrogen than in air; as can be suggested by TGA measurements from 650 °C.

When cooling in air, the temperature of the phase transition and cell parameters are strictly the same than when heating (Fig. 2a and b). In nitrogen, the phase transition from rhombohedral to monoclinic phase occurs at higher temperature (300–400 °C) and final lattice parameters are larger than initial ones at room temperature (Fig. 2d). The different behaviour in nitrogen is attributed to the oxygen loss from the material on heating which is not reversible on cooling (Fig. 4).

Some authors have observed a similar behaviour in the case of $La_{1-x}Sr_xFeO_{3-\delta}$ materials and more particularly for LSF 821.[19,20] On heating, they have observed a phase transition from orthorhombic to rhombohedral symmetry in the case of LSF 821 and an anisotropic thermal expansion during the orthorhombic phase. In this case, *b*- and *c*-lattice parameters exhibit larger TECs than *a*-lattice parameter. As for LSFG 8273, we can assume that this anisotropy increases the distortion of the FeO_6 octahedrons.

3.2. Thermal expansion behaviour

Expansion behaviour data provide macroscopic measurements of thermal expansion of materials compared to XRD, but on a wider range of temperature.

Fig. 5 shows the dimensional behaviour of LSFG 8273 and LSF 821 materials submitted to air and nitrogen atmospheres from room temperature to 1100 °C.

Under air, thermal expansion is fully reversible for the two materials in agreement with XRD analysis. This behaviour is correlated with the reversible exchange of oxygen previously observed on TGA curves (Fig. 4).

Under nitrogen, the thermal expansion of LSFG 8273 and LSF 821 is not reversible on cooling. This can be explained by the inability of the materials to recover the quantity of oxygen lost during heating (Fig. 4).

Three thermal expansion coefficients can be measured, for both materials, from the dilatometric curves for different ranges of temperature (Table 4).

The drop in thermal expansion coefficient, beginning around 270 °C and ending at 320 °C for LSFG 8273, corresponds to the phase transition already highlighted.[21] This phase transition occurs exactly at the same temperature in air and in nitrogen. The atmosphere does not have any influence on thermal expansion up to 850 °C before and after phase transition (Table 4).

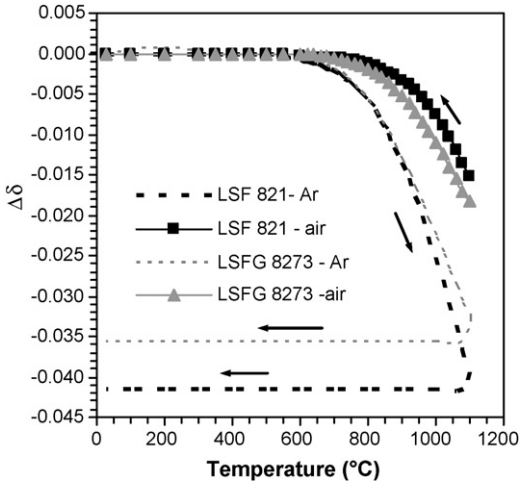

Fig. 4. Oxygen vacancies concentrations of LSF 821 and LSFG 8273 in air and neutral atmosphere in order to temperature.

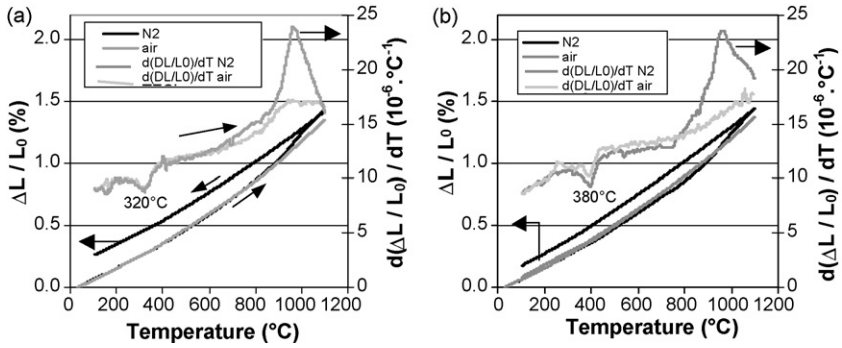

Fig. 5. Thermal expansion coefficient and dilatation of both (a) LSFG 8273 and (b) LSF 821 in air and nitrogen.

In the case of LSF 821, a drop in thermal expansion coefficient is also observed, beginning at 340 °C. There is a shift of temperature compared to LSFG 8273. This can be attributed to the orthorhombic-to-rhombohedral phase transition. Tai et al. have studied a similar phase transition on $La_{1-x}Sr_xCo_{1-y}Fe_yO_3$ materials.[20,22] They observed that the temperature of the phase transition is strongly dependent on the contents of Sr^{2+} and Co^{3+}. The phase transition temperature increases with lowering Co^{3+} content and reaches its maximal value for LSF 821. So the difference of the phase transition temperature between the two materials can be explained by the substitution of iron by gallium.

In all cases, the rhombohedral phase exhibits a coefficient of thermal expansion higher than the low temperature phase (monoclinic in the case of LSFG 8273 and orthorhombic in the case of LSF 821).

At high temperature (i.e. above 850 °C), the expansion increases under air and nitrogen atmospheres (Table 4). That is directly linked to the greater weight loss observed on TGA curves. Some authors have highlighted a "chemically induced expansion" added to classical thermal expansion above a T^* temperature (~850 °C), due to oxygen loss .[6,8,23,24] Departure of oxygen from the material in air and neutral atmospheres causes cell expansion, due to both cationic repulsion and reduction of Fe^{4+} (0.58 Å) to Fe^{3+} (0.64 Å). In air, both materials exhibit a similar thermal expansion. In nitrogen, both materials present greater weight losses than in air and higher TECs. That is in good agreement with the chemically induced expansion, attributed to oxygen departure from the perovskite structure. This chemical expansion is linked with absolute oxygen non-stoichiometry of perovskite material which is presented in recent works.[25,26] Moreover, replacing iron cations by gallium cations will decrease the effect of iron on thermal expansion and lead to a lower TEC for LSFG 8273 than for LSF 821. As the dense membrane is exposed to a gradient of oxygen partial pressure, mismatch in expansion of the material submitted to air and inert or reducing atmosphere at high temperature is strongly limited by introducing gallium on the B-site.[6,8] It can be noted that cell expansion occurs at lower temperature on XRD data than on dilatometric curves, probably due to the use of powders for XRD analysis instead of a monolithic samples for dilatometric measurements.

Table 4
Thermal expansion coefficient of LSF 821 and LSFG 8273 materials in air and nitrogen.

	TEC in air (10^{-6} °C^{-1})	TEC in nitrogen (10^{-6} °C^{-1})
LSFG 8273	9.7 (RT–320)	9.5 (RT–320)
	12.4 (320–850)	12.4 (320–850)
	16.8 (850–1100)	20.6 (850–1100)
LSF 821	10.3 (RT–380)	10.0 (RT–380)
	13.2 (380–850)	13.1(380–850)
	16.2 (850–1100)	21.5 (850–1100)

3.3. Young's modulus

Young's modulus was measured vs. temperature up to 1100 °C for samples sintered in air with a relative density of at least of 96% of the theoretical density. Fig. 6 shows the variations with temperature of the elastic moduli of both dense LSFG 8273 and LSF 821 in air and nitrogen. As relative densities of the samples are not totally equal, data are corrected to take into account the porosity using a linear law $E_0 = E/(1-2P)$ with E the measured Young's modulus and P the evaluated porosity of the material.[27]

At room temperature, LSF 821 is about 30% stiffer than LSFG 8273, which is probably due to the iron substitution by gallium. This phenomenon may be associated with (i) the significant difference in the covalence of Fe–O and Ga–O bonds and (ii) the lattice distortion induced by Ga doping. Indeed, Ga–O bond energy is lower than for Fe–O one that can involve a softening of the material as Young's modulus is directly linked to bond energies. Moreover, Ga doping leads to a cell distortion, as LSF 821 and LSFG 8273 can be refined respectively into orthorhombic and monoclinic structures, and this involves local lattice distortion implying a decrease of stiffness.[8,21,24,28]

For LSFG 8273, under both air and nitrogen up to T1 (270 °C) Young's modulus decreases by approximatively 33% of the initial value. An increase of 15% on the basis of the minimal value (T1) is observed up to T2 (860 °C in air and 800 °C in nitrogen). Then, up to T3 (1100 °C), E decreases by about 3.5% in air and 5% in nitrogen on the basis of the T2 value.

A similar behaviour is observed for LSF 821 dense material. Up to 340 °C (T1) Young's modulus is decreasing of about 38% of the initial value. Then it increases of 19% from the minimal

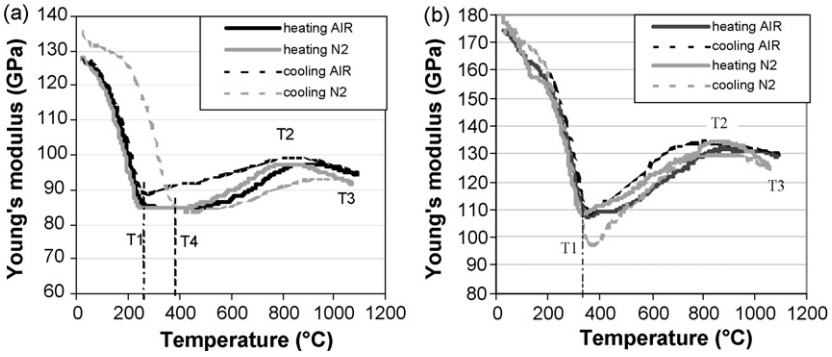

Fig. 6. Young's modulus of (a) LSFG 8273 and (b) LSF 821 under air and nitrogen.

value up to 800 °C (T2) and decreases again of 3% in air and 7% in nitrogen above this temperature.

On heating, the two materials exhibit similar behaviours under air and nitrogen with three stages in the Young's modulus evolution as a function of the temperature: (i) from room temperature to T1, (ii) between T1 and T2 and (iii) over T2.

From room temperature to T1, the strong decrease of the elastic moduli can be attributed to the slight variation of elastic constants (C_{ij}) of the low temperature phase. More data are needed to confirm this supposed origin of the drop of the Young's modulus. Nevertheless, Young's modulus is very sensitive to crystal lattice variation.[29] In the case of LSF 821, an increase of the FeO_6 octahedrons distortion between room temperature and T1, due to an anisotropy in the evolution with temperature of lattice parameters, was confirmed by Fossdal et al.[19] Same anisotropy and BO_6 octahedron distortion is observed by HTXRD, between room temperature and T1, for LSFG 8273. This rise of the distortion results in the softening of two Fe–O bonds (Table 3), as discussed previously, that could explain the drop of the Young's modulus in both LSF 821 and LSFG 8273. Some authors have already underlined the influence of the BO_6 octahedron distortion on the Young's modulus of perovskite materials such as $La_{1-x}Ca_xMnO_3$.[30] They showed that the magnitude of the drop of the Young's modulus is correlated to the type of distortion of the BO_6 octahedrons. When the fraction of Q_3-type distortion (elongated mode) increases, the magnitude of the drop of the Young's modulus increases, conversely when the fraction of Q_2-type distortion (compressed mode) increases. No Jahn–Teller effect is present in the $LaFeO_3$ perovskites as Fe^{3+} is an octahedrally symmetric ion,[31] however doping with Ga modifies bond lengths of FeO_6 octahedron. So the distortion of the BO_6 octahedron could explain why LSF 821 exhibits a greater drop of Young's modulus.

Cell distortions are observed on LSF 821 and LSFG 8273, so we can assume that cell distortion, especially for the octahedron, leads to a decrease of Young's modulus observed from room temperature to T1 under both atmospheres.

Then around T1, phase transition from the low temperature phase to rhombohedral symmetry occurs according to XRD and dilatometric data. The phase transition is associated with a stiffening of the material, resulting in a minimum of Young's modulus.[32] The increase of Young's modulus between T1 and T2 may be due to the less distorted BO_6 octahedron as all Fe–O bonds are identical in the rhombohedral phase.[33,34]

During the third stage over T2, the slight decrease of E values corresponds to a weight loss of the material and a strong increase in thermal expansion under both atmospheres. The oxygen departure from the perovskite structure implies a cell expansion with a weakening of the rigidity. The decrease of Young's modulus is greater in nitrogen due to the larger oxygen loss (Fig. 4).

On cooling, the same three stages are observed under both atmospheres. Transition temperatures are similar except for LSFG 8273 under nitrogen atmosphere. For the latter, phase transition occurs at a temperature T4 (380 °C) higher on cooling than on heating (270 °C), probably due to impossible oxygen recovery. Moreover, final Young's modulus of LSFG 8273 in nitrogen is higher than the initial value, whereas in air, final and initial values are equal. The high temperature XRD measurements have shown that after treatment at 900 °C during 10 h in air LSFG 8273 material exhibits similar cell parameters to the initial ones while under nitrogen the lattice parameters are higher and β is lower than the initial value (90.01°). This induces a slight diminution of the cell distortion, becoming almost orthorhombic, which can explain the increase in Young's modulus on cooling. For LSFG 8273 in air and LSF 821 under both atmospheres, the evolution of Young's modulus is totally reversible with temperature.

From other considerations, these two types of materials are likely to exhibit a ferroelastic behaviour. Young's modulus evolution with respect to temperature could be dependent on the difference of ferroelastic behaviour of orthorhombic or monoclinic and the rhombohedral phase. In this way, Fossdal et al. and Orlovskaya et al. have shown that $LaFeO_3$,[35] $LaCoO_3$ and $La_{0.8}Ca_{0.2}CoO_3$ perovskites[36,37] present a ferroelastic behaviour with orthorhombic–rhombohedral phase transition. Besides, Young's modulus evolution of LSFG8273 and LSF821 perovskites with temperature between 25 °C and 600 °C is similar to Young's modulus evolution of $LaCoO_3$ perovskites presented by Orlovskaya et al.[36,37] The ferroelastic behaviour of LSFG8273 and LSF821 perovskites could be expected above the orthorhombic-to-rhombohedral phase transition described in this study by analogy with $LaCoO_3$ and $La_{0.8}Ca_{0.2}CoO_3$ perovskites. However, this ferroelastic

behaviour does not explain clearly the increase of Young's modulus with temperature between 400 °C and 600 °C, and leads to a nonlinear stress–strain relationship which should be confirmed by a complementary microstructural analysis and mechanical tests in further studies, such as bending or compressive tests.

The differences observed between heating and cooling stages under nitrogen and air for LSFG 8273 suggest possible stress development in the membrane under working conditions and more particularly, during cooling stage, as one face of the membrane will be exposed to air and the other one to reducing conditions. So for industrial applications, temperature and atmosphere have to be controlled during cooling step to avoid cracking of the membrane.

4. Conclusions

The thermal behaviour of $La_{0.8}Sr_{0.2}FeO_{3-\delta}$ and $La_{0.8}Sr_{0.2}Fe_{0.7}Ga_{0.3}O_{3-\delta}$ was studied between room temperature and 1100 °C. The two materials are meant to be respectively the porous support and the dense membrane of a catalytic membrane reactor. Both materials must exhibit similar thermal expansions and good mechanical properties. Structural, thermogravimetric and dilatometric analyses associated with Young's modulus measurements were performed over a large range of temperature under air and nitrogen to give a qualitative description of the thermal behaviour of both materials.

These measurements show that LSF 821 is stiffer than LSFG 8273 respectively 170 GPa and 120 GPa at room temperature. This result is probably linked to the introduction of Ga in the perovskite structure, leading to local lattice distortion and to softening.[24] Both LSFG 8273 and LSF 821 exhibit a phase transition respectively at 270 °C and 340 °C resulting in a minimal value of Young's modulus. It is assumed that the strong decrease of Young's modulus before phase transition is due to an increased cell distortion. After phase transition, both materials exhibit a rhombohedral phase with higher TECs and Young's modulus values. Then over 850 °C, oxygen departure from the perovskite structure observed on TGA measurements, involves a strong rise of the thermal expansion and a small Young's modulus decrease.

The evolution of Young's modulus with temperature was identified as a very important parameter in term of stress development in the membrane. These results show that expansion behaviour and the evolution of mechanical properties of those materials are of great importance to improve the reliability of catalytic membrane reactors.

Acknowledgements

The authors would like to thank Mme C. Pirovano (UCCS, Lille, France) for High Temperature XRD measurements and corresponding Rietveld refinement, M. Huger (GEMH, Limoges, France) for fruitful discussions and D.S. Smith for his previous work about thermo-mechanical behaviour of ceramic materials.

The authors want to express their gratitude to Air Liquide for supporting this research.

References

1. Rostrup-Nielsen, J. R., Catalysis and large-scale conversion of natural gas. *Catal. Today*, 1994, **21**, 257.
2. Rostrup-Nielsen, J. R., New aspects of syngas production and use. *Catal. Today*, 2000, **63**, 159.
3. Sammells, A. F., Schwartz, M., Mackay, R. A., Barton, T. F. and Peterson, D. R., Catalytic membrane reactors for spontaneous synthesis gas production. *Catal. Today*, 2000, **56**, 325.
4. Bouwmeester, H. J. M., Dense ceramic membranes for methane conversion. *Catal. Today*, 2003, **82**, 141.
5. Kharton, V. V., Patrakeev, M. V., Waerenborgh, J. C., Sobyanin, V. A., Veniaminov, S. A., Yaremchenko, A. A. *et al.*, Methane oxidation over perovskite-related ferrites: effects of oxygen nonstoichiometry. *Solid State Sci.*, 2005, **7**, 1344.
6. Kharton, V. V., Shaulo, A. L., Viskup, A. P., Avdeev, M., Yaremchenko, A. A., Patrakeev, M. V. *et al.*, Perovskite-like system (Sr, La)(Fe, Ga)$O_{3-\delta}$: structure and ionic transport under oxidizing conditions. *Solid State Ionics*, 2002, **150**, 229.
7. Kharton, V. V., Yaremchenko, A. A., Kovalevsky, A. V., Viskup, A. P., Naumovich, E. N. and Kerko, P. F., Perovskite-type oxides for high-temperature oxygen separation membranes. *J. Membr. Sci.*, 1999, **163**, 307.
8. Kharton, V. V., Yaremchenko, A. A., Patrakeev, M. V., Naumovich, E. N. and Marques, F. M. B., Thermal and chemical induced expansion of $La_{0.3}Sr_{0.7}$(Fe,Ga)$O_{3-\delta}$ ceramics. *J. Eur. Ceram. Soc.*, 2003, **23**, 1417.
9. Naumovich, E. N., Patrakeev, M. V., Kharton, V. V., Islam, M. S., Yaremchenko, A. A., Frade, J. R. *et al.*, Defect interactions in $La_{0.3}Sr_{0.7}Fe(M')O_{3-\delta}$ (M′ = Al, Ga) perovskites: atomistic simulations and analysis of $p(O_2)$-T-δ diagrams. *Solid State Ionics*, 2006, **177**, 457.
10. Patrakeev, M. V., Bahteeva, J. A., Mitberg, E. B., Leonidov, I. A., Kozhevnikov, V. L. and Poeppelmeier, K. R., Electron/hole and ion transport in $La_{1-x}Sr_xFeO_{3-\delta}$. *J. Solid State Chem.*, 2003, **172**, 219.
11. Teraoka, Y., Oxygen permeation through perovskite-type oxides. *Chem. Lett.*, 1985, **14**, 1743.
12. Teraoka, Y., Zhang, H. M., Okamoto, K. and Yamazoe, N., Mixed ionic–electronic conductivity of $La_{1-x}Sr_xCo_{1-y}Fe_yO_{3-\delta}$ perovskite-type oxides. *Mater. Res. Bull.*, 1988, **23**, 51.
13. Blond, E. and Richet, N., Thermomechanical modelling of ion-conducting membrane for oxygen separation. *J. Eur. Ceram. Soc.*, 2008, **28**, 793.
14. Etchegoyen, G., Chartier, T. and Del-Gallo, P., An architectural approach to the oxygen permeability of a $La_{0.6}Sr_{0.4}Fe_{0.9}Ga_{0.1}O_{3-\delta}$ perovskite membrane. *J. Eur. Ceram. Soc.*, 2006, **26**, 2807.
15. Baudson, H., Debucquoy, F., Huger, M., Gault, C. and Rigaud, M., Ultrasonic measurement of Young's modulus MgO/C refractories at high temperature. *J. Eur. Ceram. Soc.*, 1999, **19**, 1895.
16. Holc, J., Kuscer, D., Hrovat, M., Bernik, S. and Kolar, D., Electrical and microstructural characterisation of $(La_{0.8}Sr_{0.2})(Fe_{1-x}Al_x)O_3$ and $(La_{0.8}Sr_{0.2})(Mn_{1-x}Al_x)O_3$ as possible SOFC cathode materials. *Solid State Ionics*, 1997, **95**, 259.
17. Kuscer, D., Holc, J., Hrovat, M. and Kolar, D., Correlation between the defect structure, conductivity and chemical stability of $La_{1-y}Sr_yFe_{1-x}Al_xO_{3-\delta}$ cathodes for SOFC. *J. Eur. Ceram. Soc.*, 2001, **21**, 1817.
18. Woodward, P., Octahedral tilting in perovskites. I. Geometrical considerations. *Acta Crystallogr. B*, 1997, **53**, 32.
19. Fossdal, A., Menon, M., Wærnhus, I., Wiik, K., Einarsrud, M. A. and Grande, T., Crystal structure and thermal expansion of $La_{1-x}Sr_xFeO_{3-\delta}$ materials. *J. Am. Ceram. Soc.*, 2004, **87**, 1952.
20. Tai, L. W., Nasrallah, M. M., Anderson, H. U., Sparlin, D. M. and Sehlin, S. R., Structure and electrical properties of $La_{1-x}Sr_xCo_{1-y}Fe_yO_3$. Part 1. The system $La_{0.8}Sr_{0.2}Co_{1-y}Fe_yO_3$. *Solid State Ionics*, 1995, **76**, 259.
21. Hayashi, H., Suzuki, M. and Inaba, H., Thermal expansion of Sr- and Mg-doped $LaGaO_3$. *Solid State Ionics*, 2000, **128**, 131.
22. Tai, L. W., Nasrallah, M. M., Anderson, H. U., Sparlin, D. M. and Sehlin, S. R., Structure and electrical properties of $La_{1-x}Sr_xCo_{1-y}Fe_yO_3$.

Part 2. The system $La_{1-x}Sr_xCo_{0.2}Fe_{0.8}O_3$. *Solid State Ionics*, 1995, **76**, 273.
23. Kharton, V. V., Sobyanin, V. A., Belyaev, V. D., Semin, G. L., Veniaminov, S. A., Tsipis, E. V. *et al.*, Methane oxidation on the surface of mixed-conducting $La_{0.3}Sr_{0.7}Co_{0.8}Ga_{0.2}O_{3-\delta}$. *Catal. Commun.*, 2004, **5**, 311.
24. Yaremchenko, A. A., Kharton, V. V., Shaula, A. L., Patrakeev, M. V. and Marques, F. M. B., Transport properties and thermal expansion of perovskite-like $La_{0.3}Sr_{0.7}Fe(Al,Cr)O_{3-\delta}$ ceramics. *J. Eur. Ceram. Soc.*, 2005, **25**, 2603.
25. Søgaard_, M., Hendriksen, P. V. and Mogensen, M., Oxygen nonstoichiometry and transport properties of strontium substituted lanthanum ferrite. *J. Solid State Chem.*, 2007, **180**, 1489–1503.
26. Yaremchenko, A. A., Kharton, V. V., Patrakeev, M. V. and Marques, F. M. B., Oxygen ionic and electronic conductivity of $La_{0.3}Sr_{0.7}Fe(Al)O_3$-[delta] perovskites. *Solid State Sci.*, 2004, **6**, 357.
27. Glandus, J. C., *Rupture fragile et résistance aux chocs thermiques de céramiques à usage mécanique*. Université de Limoges, 1981.
28. Patrakeev, M. V., Mitberg, E. B., Lakhtin, A. A., Leonidov, I. A., Kozhevnikov, V. L., Kharton, V. V. *et al.*, Oxygen nonstoichiometry, conductivity, and seebeck coefficient of $La_{0.3}Sr_{0.7}Fe_{1-x}Ga_xO_{2.65+\delta}$ perovskites. *J. Solid State Chem.*, 2002, **167**, 203.
29. Okamura, T., Shimizu, S., Mogi, M., Tanimura, M., Furuya, K. and Munakata, F., Elastic properties of Sr- and Mg-doped lanthanum gallate at elevated temperature. *J. Power Sources*, 2004, **130**, 38.
30. Ma, Y. Q., Song, W. H., Yang, J., Zhang, R. L., Zhao, B. C., Sheng, Z. G. *et al.*, The current-induced effect on the Jahn–Teller distortion in the $La_{0.5}Ca_{0.5}MnO_3$ manganite. *Solid State Commun.*, 2005, **133**, 163.
31. Lufaso, M. W. and Woodward, P. M., Jahn–Teller distortions, cation ordering and octahedral tilting in perovskites. *Acta Crystallogr. B*, 2004, **60**, 10.
32. Suasmoro, S., Smith, D. S., Lejeune, M., Huger, M. and Gault, C., High temperature ultrasonic characterization of intrinsic and microstructural changes in ceramic $YBa_2Cu_3O_{7-\delta}$. *J. Mater. Res.*, 1992, **7**, 1629.
33. Slater, P. R., Irvine, J. T. S., Ishihara, T. and Takita, Y., High-temperature powder neutron diffraction study of the oxide ion conductor $La_{0.9}Sr_{0.1}Ga_{0.8}Mg_{0.2}O_{2.85}$. *J. Solid State Chem.*, 1998, **139**, 135.
34. Zheng, G. H., Sun, Y. P., Zhu, X. B. and Song, W. H., Transport, magnetic, internal friction, and Young's modulus in the Y-doped manganites $La_{0.9-x}Y_xTe_{0.1}MnO_3$. *J. Solid State Chem.*, 2006, **179**, 1394.
35. Fossdal, A., Einarsrud, M.-A. and Grande, T., Mechanical properties of $LaFeO_3$ ceramics. *J. Eur. Ceram. Soc.*, 2005, **25**, 927.
36. Orlovskaya, N., Lugovy, M., Pathak, S., Steinmetz, D., Lloyd, J., Fegely, L. *et al.*, Thermal and mechanical properties of $LaCoO_3$ and $La_{0.8}Ca_{0.2}CoO_3$ perovskites. *J. Power Sources*, 2008, **182**, 230.
37. Orlovskaya, N., Browning, N. and Nicholls, A., Ferroelasticity in mixed conducting $LaCoO_3$ based perovskites: a ferroelastic phase transition. *Acta Mater.*, 2003, **51**, 5063.